Online ISSN: 2981-0396 Print ISSN: 2981-0388

International Journal of Iron & Steel Society of Iran

Journal Homepage: https://journal.issiran.com/

Research Article

Predicting Metallurgical Length in Continuous Casting Using Machine Learning

H. Safaei *[1], B. Asadi [2]

Mechanical Engineering Group, Golpayegan College of Engineering, Isfahan University of Technology

ARTICLE INFO

Keywords:

Continouse Casting, Suppor Vector Machines, Numerical Simulation.

Article history:

Received 25 January 2025
Received in revised form 29 January 2025
Accepted 05 August 2025

ABSTRACT

This study investigates the application of machine learning, specifically Support Vector Machines (SVM), to predict the metallurgical length in continuous casting. The metallurgical length, defined as the distance from the molten metal surface to the point of complete solidification, significantly impacts product quality. Traditional methods for predicting metallurgical length, such as the K-factor model and numerical simulations, face limitations in accuracy, computational cost, and adaptability to real-time industrial applications. To address these limitations, this study proposes a novel approach using Support Vector Machines (SVM), a machine learning algorithm, to predict metallurgical length with high precision. Numerical simulations were conducted to model fluid flow, heat transfer, and solidification processes, validated against experimental data. The SVM model was trained on metallurgical length data derived from simulations at various casting speeds. Results demonstrated that the SVM model achieved a mean square error (MSE) of 0.0789 compared to numerical data, significantly outperforming empirical methods (MSE = 0.5353). The study highlights the potential of machine learning to enhance real-time decision-making in continuous casting, offering a computationally efficient and accurate alternative to traditional methods. This approach can be extended to analyze other process parameters, such as cooling water flow rate and initial superheat temperature, further optimizing steel production.

1. Introduction

In recent years, continuous casting has emerged as the dominant steel production method, accounting for over 95% of global steel output. This process involves the transformation of molten metal into solid slabs through a continuous and highly controlled procedure. One of the critical parameters in continuous casting is the metallurgical length, defined as the distance from the free surface of the molten metal in the mold to the point where the metal achieves complete solidification [1]. Accurate determination and optimization of the metallurgical length are essential for ensuring the quality and integrity of the final product.

The production of specialty steels, in particular, places stringent demands on continuous casting processes. A key requirement is the optimization of product quality, which can be achieved through advanced systems such as the Dynamic Soft Reduction (DSR) system. The DSR system plays a pivotal role in mitigating defects such as slab segregation and internal voids, which are among the

* *Corresponding Author*
Email: h.safaei@iut.ac.ir
Address: Mechanical Engineering Group, Golpayegan College of Engineering, Isfahan University of Technology
1. Assistant Professor, 2. Assistant Professor

DOI: http://10.22034/IJISSI.2025.2051653.1317
Published by ISSI (Iron & Steel Society of Iran)

most significant challenges in the production of high-grade steels [2]. For the DSR system to operate effectively, precise control of the cooling process and accurate calculation of the metallurgical length are imperative [3]. Achieving this level of precision, however, is not without its challenges. The definition of "complete solidification" can vary depending on the specific application, influencing the choice of measurement techniques or predictive models. While various laboratory methods exist for determining the metallurgical length, many of these approaches are costly and require continuous calibration of measurement tools. As a result, mathematical models have become a preferred alternative for predicting the metallurgical length.

One of the most widely recognized mathematical models for this purpose is the "K-factor" model, expressed as [1]:

$$s = K\sqrt{t} \qquad \text{Eq.(1)}$$

where s represents the thickness of the solidified section, t denotes the solidification start time, and K is a constant coefficient dependent on factors such as steel grade, initial superheat temperature, and cooling water flow rate [1]. Despite its widespread use, the K-factor model has inherent limitations. For instance, steel during solidification consists of three distinct regions-liquid, solid, and mushy zones-each requiring different 'K' coefficients. Therefore, different 'K' values are necessary for various conditions in practical applications.

To address these limitations, researchers have turned to more sophisticated approaches, such as numerical methods. Numerical simulations offer a more accurate representation of the continuous casting process by incorporating fewer assumptions and better capturing the underlying physics. These methods provide detailed insights into the solidification process and enable precise predictions of the metallurgical length. However, their computational intensity and high time costs pose significant challenges, particularly in industrial settings where rapid decision-making is crucial.

In recent years, machine learning (ML) has emerged as a promising solution to overcome the limitations of traditional numerical methods. By leveraging data generated from numerical simulations, machine learning algorithms can be trained to predict key parameters, such as the metallurgical length, with remarkable accuracy and efficiency. This approach not only reduces computational costs but also enables real-time decision-making, offering a highly attractive solution for industrial applications where speed and precision are critical.

Many researchers have employed numerical methods to simulate continuous casting; however, the application of machine learning techniques in this area remains limited. Chen et al. [3] investigated spray-cooling control in steel continuous casting, with a focus on maintaining a consistent metallurgical length during variations in casting speed. The study analyzed four control strategies to evaluate their effectiveness, identifying the bang-bang control method as the most effective. This method was shown to reduce metallurgical length dips to less than 1 meter. However, its effectiveness was limited during sudden speed drops. During steady casting, the metallurgical length was consistently maintained at 22.29 meters. The study also emphasized that abrupt changes in casting speed should be avoided to ensure process stability. Milkowska and Falkus [4] conducted a comprehensive review of numerical models for steel continuous casting, with a particular focus on heat transfer and solidification processes. The study examined the accuracy of boundary and initial conditions and employed sensitivity analysis to evaluate the influence of input parameters on output results. Additionally, various heat transfer coefficient models were compared to identify the most effective approaches.

Li et al. [5] elaborated on the fundamental principles underlying mechanisms for identifying sticking breakout predictions, aiming to detect abnormal temperature patterns. These principles emphasize monitoring mold friction, analyzing individual thermocouple temperature patterns, examining horizontal groups of thermocouples, and integrating these observations into dynamic fuzzy neural networks (NNs). Cheng et al. [6] proposed a compound sticking breakout prediction model that incorporates both the time-sequence analysis of individual thermocouples and a spatial module for groups of thermocouples. This integrated approach enhances the accuracy of sticking breakout detection. He and Zhang [7] proposed a novel breakout prediction method that integrates a genetic algorithm-optimized backpropagation neural network (GA-BPNN) with logical rules. This approach achieved a 100% detection ratio during field tests while significantly reducing the false alarm frequency to 0.1365%. By improving the precision of recognizing sticking temperature patterns, the method effectively addresses key challenges associated with high-speed continuous casting technology. The combination of GA-BPNN and logical rules enhances both time-series and spatial modeling capabilities, facilitating the accurate identification of sticker- breakout. Lu et al. [8] focused on real-time prediction in the continuous casting process by developing a deep learning model to accurately predict three-dimensional temperature fields. The model achieved a mean absolute error of 4.19 K and a mean absolute percentage error of 0.49% on test data, demonstrating high predictive accuracy. Additionally, Bayesian optimization was utilized to improve the adaptive adjustment of operating parameters, leading to enhanced manufacturing efficiency and a significant reduction in defects. Cermenek et al. [9] conducted a survey on the application of machine learning in continuous steel casting, addressing key challenges related to process monitoring and control. The study highlights the critical role of machine learning techniques

in managing the complexities of the casting process. It categorizes existing machine learning applications in the field and provides a comprehensive discussion of the challenges, proposed solutions, and potential directions for future research.

Recent advancements in the application of machine learning (ML) to continuous casting processes have predominantly focused on sticker breakouts failures. However, the accurate prediction of metallurgical length remains underexplored in the literature. This study introduces a novel methodology that leverages Support Vector Machines (SVM), a robust machine learning algorithm, to predict the metallurgical length with high precision. The SVM algorithm is particularly suited for this task due to its ability to handle high-dimensional data, generalize well to unseen cases, and deliver reliable results even with limited training datasets.

2. Mathematical Model

Numerical simulation of the casting process represents a complex and multifaceted challenge within the field of computational fluid dynamics (CFD). This complexity arises from the interplay of fluid flow dynamics, phase change from liquid to solid, and additional contributing factors that introduce significant computational demands. Accurate computational models must effectively capture the behavior of fluid flow, temperature, and the evolution of the solidifying steel shell. To determine the temperature distribution within the steel strand, it is essential to solve the transient energy equation. Considering the provided explanations, it is necessary to solve the full Navier-Stokes equations in the turbulent flow regime.

2.1. Governing Equations

The equations employed in this section have been previously validated and utilized by the authors [10].

For incompressible fluid flow, the continuity equation is expressed as:

$$\vec{\nabla}.\vec{V} = 0 \qquad \text{Eq.(2)}$$

Where $\vec{V}$ is the velocity vector of the fluid flow. The momentum equation, in its generalized form, is formulated as:

$$\frac{\partial(\rho\vec{V})}{\partial t} + \vec{\nabla}.(\rho\vec{V}\vec{V}) = -\vec{\nabla}p \qquad \text{Eq.(3)}$$

$$+\vec{\nabla}.\left(\mu\vec{\nabla}\vec{V}\right) - \vec{g}\cdot\vec{x}\nabla\rho + \vec{S}_v$$

Here, $\vec{S}_v$ denotes the source term for solidification. This term must ensure that as the steel solidifies, its velocity reduces to 0. The source term was defined by Voller [11] as:

$$\vec{S}_v = -A\vec{V} where A = \frac{-C(1-\theta)^2}{(\theta^3+\varepsilon)} \qquad \text{Eq.(4)}$$

Here θ represents the liquid fraction within the computational cell, C is a parameter dependent on the morphology of the porous medium, and ε is a small constant added to the denominator to prevent numerical instability.

To simulate turbulent flow, the k-ε turbulence model is employed. Additionally, the energy equation is utilized to model heat transfer and track the phase change boundary:

$$\frac{\partial(\rho C_p T)}{\partial t} + \vec{\nabla}\cdot(\rho C_p\vec{V}T) \qquad \text{Eq.(5)}$$

$$+\left(\frac{\partial\rho K_E}{\partial t} + \vec{\nabla}\cdot(\rho\vec{V}K_E)\right)$$

$$= -\frac{\partial P}{\partial t} + \vec{\nabla}\cdot(k\vec{\nabla}T)$$

$$+\vec{\nabla}\cdot\left(\underset{\sim}{\tau}\cdot\vec{V}\right) + \rho\vec{g}\cdot\vec{V} + S_h,$$

$$S_h = \frac{\partial\rho\Delta H}{\partial t} + \vec{\nabla}\cdot(\rho\vec{V}\Delta H)$$

$$\underset{\sim}{\tau} = \mu\left[\vec{\nabla}\vec{V} + \vec{\nabla}\vec{V}^T\right] - \frac{2}{3}\mu I\vec{\nabla}\cdot\vec{V}$$

Where K_E is kinetic energy of the fluid, $\underset{\sim}{\tau}$ is the stress tensor, k is the thermal conductivity, S_h is the solidification source term and ΔH is the latent heat of fusion.

Voller [11] proposed that within the mushy zone, the latent heat of fusion ΔH is proportional to the total latent heat of solidification L, expressed as ΔH = θL. Rösler [12] further defined the liquid fraction θ as:

$$\theta = 0.5 erf\left(\frac{4(T-T_m)}{(T_l-T_s)}\right) + 0.5 \qquad \text{Eq.(6)}$$

Where T_l and T_s represent the liquidus and solidus temperatures, respectively. Consequently, the energy equation can be reformulated as:

$$\frac{\partial(\rho C_p T)}{\partial t} + \vec{\nabla}\cdot(\rho C_p\vec{V}T) \qquad \text{Eq.(7)}$$

$$+\left(\frac{\partial\rho K_E}{\partial t} + \vec{\nabla}\cdot(\rho\vec{V}K_E)\right)$$

$$= -\frac{\partial P}{\partial t} + \vec{\nabla}\cdot(k_{eff}\vec{\nabla}T)$$

$$+\vec{\nabla}\cdot\left(\underset{\sim}{\tau}\cdot\vec{V}\right) + \rho\vec{g}\cdot\vec{V} + S_h where$$

$$S_h = -\rho L \frac{4 \cdot \left(\left(\frac{4(T - T_m)}{(T_l - T_s)} \right)^2 \right)}{(T_l - T_s)\sqrt{\pi}} \cdot$$

$$\left(\frac{\partial T}{\partial t} + \vec{V} \cdot \vec{\nabla} T \right)$$

2.2. Boundary Conditions

Molten steel is introduced into the mold through a submerged entry nozzle (SEN). For this region, the inlet boundary condition is defined by specifying the mass flow rate, which is calculated based on the casting speed, the cross-sectional area of the steel strand, and the outlet cross-sectional area of the nozzle. In the current study, the casting speed is maintained at 1 m/min. Mold oscillation was not considered in this study. A no-slip boundary condition is applied to the solid walls of the mold. In cases where a solidified shell forms on the mold wall, it is assumed to move downward at the same speed as the casting speed.

The primary cooling of the steel strand occurs within the mold, where cooling water is circulated through its four faces or panels. The average cooling rate in this region can be estimated based on the flow rate and temperature change of the cooling water, as described by the following equation:

$$\bar{q} = \frac{C_{pw} Q_m \Delta T}{S_{eff}} \quad \text{Eq.(8)}$$

Here, C_{pw} represents the specific heat capacity of water, Q_m is the flow rate of the cooling water, ΔT denotes the temperature difference between the inlet and outlet cooling water, and and S_{eff} [13] is the effective contact area between the mold and the steel strand. The heat flux distribution along the mold exhibits a decreasing trend as the casting process progresses, with the highest heat flux observed at the initial stage of the mold. This distribution is described by the following relationship:

$$q = 2680000 - \beta \sqrt{\frac{L}{u_{cast}}} \frac{J}{m^2 s} \quad \text{Eq.(9)}$$

Where:

$$\beta = \frac{1.5(2680000 - \bar{q})}{\sqrt{\frac{L}{u_{cast}}}} \quad \text{Eq(10)}$$

In these equations, L represents the distance from the free surface of the molten steel within the mold, and L_m denotes the total length of the mold. For free surfaces, a zero shear stress condition is imposed, and radiation from these surfaces is modeled with an emissivity of 0.8. At the top surface of the mold, where the molten metal interfaces with air, a zero shear stress boundary condition is also applied. These conditions ensure accurate modeling of the thermal and mechanical interactions during the casting process.

In the region outside the mold, where secondary cooling is applied, the zero shear stress condition is imposed at the free surface of the steel strand. Heat removal in this zone is predominantly achieved through water sprays. The convective heat transfer coefficient in this region is calculated using Eqs.(11) and (12) [14], depending on the cooling medium. For water-only cooling:

$$h = 165.0 W^{0.75} \quad \text{Eq.(11)}$$

For water-air mist cooling:

$$h = 350.0 W + 130 \quad \text{Eq.(12)}$$

Here, W represents the water flow rate per unit slab surface area.

3. Support Vector Machines (SVM)

Support Vector Machines (SVMs), developed by Vapnik [15] (1982, 1992, 1995, 1998) based on statistical learning theory, have been widely applied in classification, regression, and time series forecasting tasks.

Unlike methods that minimize empirical error, which may lead to reduced generalization performance, the SVM theory is based on the principle of structural risk minimization (SRM). This feature gives SVMs a significant advantage in terms of generalization performance compared to methods such as artificial neural networks (ANNs) that do not exploit this principle. In SVMs, the structural risk is a combination of the empirical error and a regularization term, as shown in the following equation:

$$R_{\text{reg}}[f] \equiv R_{\text{emp}}[f] + \frac{1}{C_s} \Omega[f] \quad \text{Eq.(13)}$$

where R_{emp} and R_{reg} represent the empirical risk and structural risk, respectively, $\|w\|^2$ is the regularization term, and C_s is the smoothing parameter that governs the trade-off between training error and model complexity. For linear problems, the decision function f(x) is defined as:

$$f(x) = \langle w, x \rangle + b \quad \text{Eq.(14)}$$

The symbol ⟨ ⟩ denotes the dot product of vectors w (the weight vector) and x (the vector of input variables). The empirical error is then derived from the following equation:

$$R_{\text{emp}}(f) = \frac{1}{m}\sum_{i=1}^{m} L(\text{y},\text{f}(x)) \qquad \text{Eq.(15)}$$

According to Vapnik's recommendation, the following error function, called ε-insensitive loss function is employed to quantify prediction errors. The mathematical formulation of this loss function is presented in Eq.(10). This function can be visualized as shown in Fig. 1.:

$$L\big(\text{y},\text{f}(x)\big) = |y - f(x)|_{\varepsilon} = \qquad \text{Eq.(16)}$$

$$\begin{cases} 0 & \text{if} \quad |y - f(x)| \le \varepsilon \\ |y - f(x)| - \varepsilon & \text{otherwise} \end{cases}$$

Fig. 1. illustrates the ϵ-insensitive loss function, which ignores errors smaller than ϵ and linearly penalizes larger deviations.

The SRM objective (Eq.(13)) is reformulated as a constrained convex optimization problem using Lagrange multipliers. The primal Lagrangian is expressed as:

$$\text{Max.} \quad \begin{cases} -\frac{1}{2}\sum_{\text{i,j=1}}^{m} (\alpha_i^* - \alpha_i)(\alpha_j^* - \alpha_j)\langle x_i, \text{x}_j\rangle \\ -\varepsilon\sum_{i=1}^{m}(\alpha_i^* + \alpha_i) + \sum_{i=1}^{m} y_i(\alpha_i^* - \alpha_i) \end{cases} \qquad \text{Eq.(17)}$$

$$\text{subject to:} \sum_{i=1}^{m}(\alpha_i - \alpha_i^*) = 0 \text{ and } \alpha_i, \alpha_i^* \in [0, \frac{C}{m}]$$

Solving this yields the optimal weight vector w and decision function f(x):

$$w = \sum_{i=1}^{m}(\alpha_i^* - \alpha_i)x_i \qquad \text{Eq.(18)}$$

$$f(x) = \sum_{i=1}^{m}(\alpha_i^* - \alpha_i)\langle x_i, \text{x}\rangle + b \qquad \text{Eq.(19)}$$

For nonlinear regression, the linear SVM framework is extended using kernel functions. The radial basis function (RBF) kernel, widely adopted for its performance, is defined as:

$$K(\text{x},\text{z}) = \exp\left(-\frac{\|x - z\|^2}{2\sigma^2}\right); \qquad \frac{1}{2\sigma^2} = \gamma \qquad \text{Eq.(20)}$$

Here, γ controls the kernel's bandwidth. Replacing the dot product $\langle x_i , x_j\rangle$ with $K(x_i , x_j)$ enables nonlinear mapping. The accuracy of SVM models critically depends on the selection of hyperparameters C, ϵ, and γ, which balance model complexity, error tolerance, and kernel sensitivity. For a comprehensive discussion of SVM theory, readers are directed to Reference [16].

4. Results

In this section, numerical simulations are conducted to analyze fluid flow and heat transfer rates. To ensure the validity and reliability of the numerical approach, the simulation outcomes are compared with the data previously reported by Shamsi and Ajmani [17]. Among the various parameters, the metallurgical length serves as a critical benchmark for comparing the results of the current study with those of the aforementioned research. Specifically, the metallurgical lengths determined in Shamsi's study [17] and the present work are 19.3 m and 19.6 m, respectively, indicating a negligible difference of only 0.3 m. Furthermore, Fig. 2. illustrates

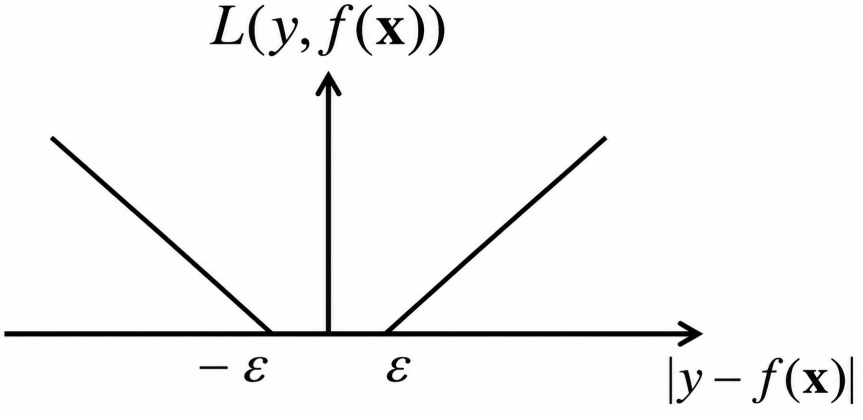

Fig. 1. The ε-insensitive loss function.

a comparative analysis of temperature variations at the strand's centerline. The minimal discrepancies observed between the two sets of results substantiate the accuracy and credibility of the present simulation.

Fig. 3. and Fig. 4. schematically illustrate the computational domain in the mold region (primary cooling zone) and the secondary cooling zone, respectively.

The computational domain was discretized using 2.5 million elements. Mesh independence was verified through multiple simulations to ensure the results are unaffected by grid resolution. The slab thickness is 200 mm. Only half of the solution domain is modeled because of the symmetry of the problem. Table 1. lists the steel properties and the values used in the numerical simulation.

The secondary cooling zone consists of 10 zones, labeled as Zone I to Zone X. The convective heat transfer coefficients for these zones are provided in Table 2. The absence of heat transfer coefficient values in the table indicates that only radiative heat transfer occurs in those zones.

Fig. 5. illustrates the temperature variations across the steel strand along longitudinal lines on the wide and narrow faces at a casting speed of 1 m/min (refer to Width and Thickness lines in Fig. 4. which extends to the end of the casting machine).

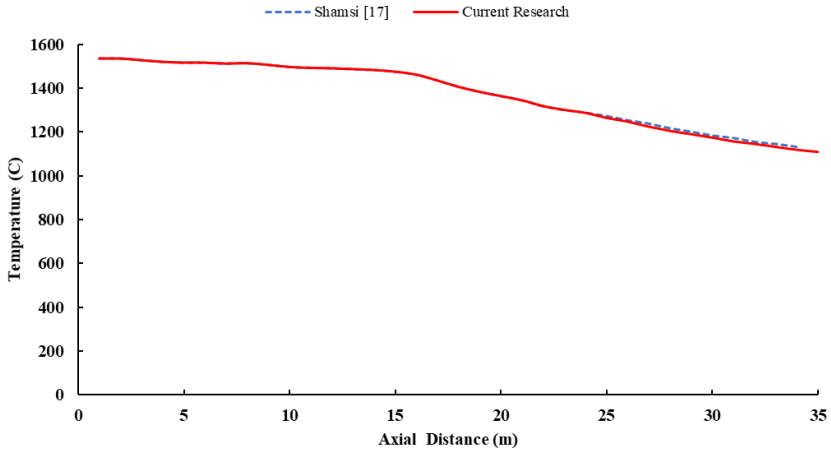

Fig. 2. Comparison of temperature variations along the line passing through the surface center of the slab in the present study and Shamsi's research [17].

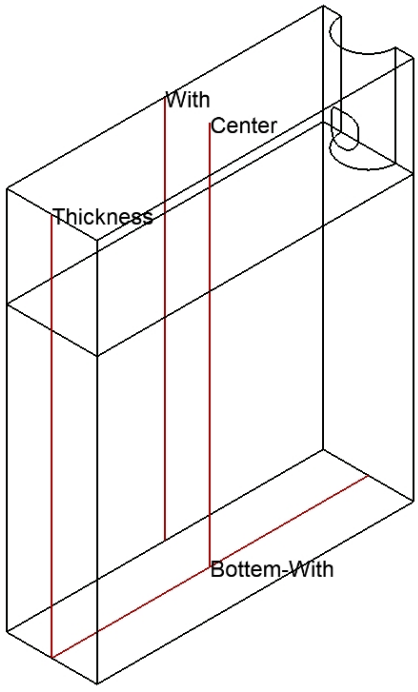

Fig. 3. Schematic of the computational domain in the mold region (primary cooling zone).

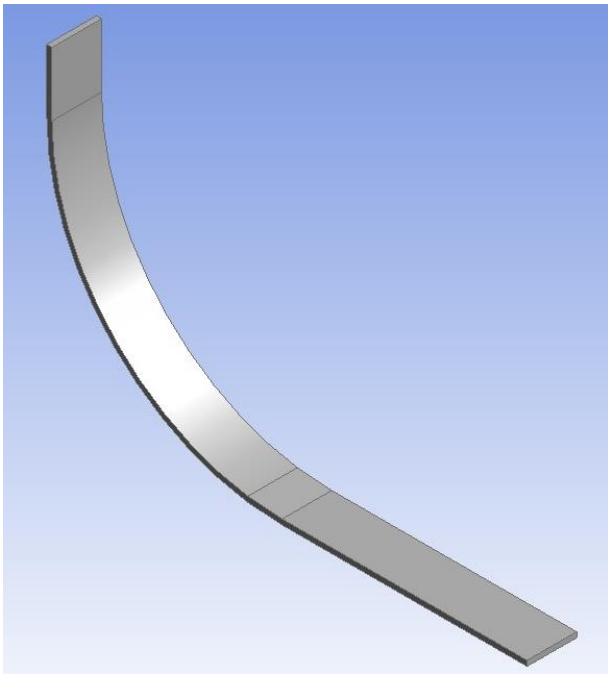

Fig. 4. Schematic of the computational domain secondary cooling zone.

Table 1. Properties of steel and values used in the numerical simulation.

Variable	Values
Thermal conductivity of steel (W/m.K)	34.6
Viscosity of steel (kg/m.s)	0.0062
Latent heat of solidification (J/kg)	271954
Solidus temperature ($^{\circ}C$)	1496
Liquidus temperature ($^{\circ}C$)	1529
Melt superheat ($^{\circ}C$)	24
Specific heat of steel ($J/kg.^{\circ}C$)	682
Length of the casting mold (m)	0.85
Strand cross-sectional area ($\mathrm{m}\times\mathrm{m}$)	1.4×0.2
SEN diameter (m)	0.12

Table 2. Heat Transfer Coefficients in Different Zones (W/m²·K).

Zone	I	II	III	IV	V	VI	VII	VIII	IX	X
	862	626	527	379	379	320	-	-	-	-

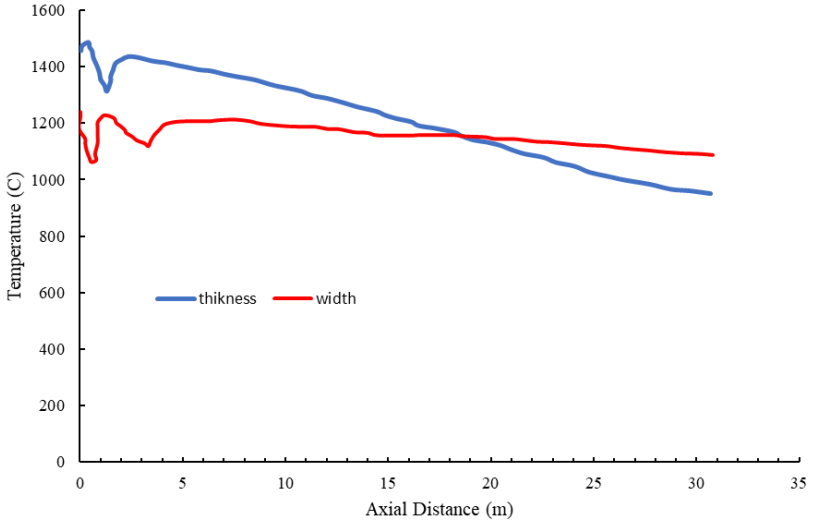

Fig. 5. Temperature variations in the wide and narrow steel strand along the longitudinal lines.

As shown, the temperature variations in the wide and narrow sections of the strand follow a similar trend. The temperature variations in the wide part of the steel strand are very significant, and the average temperature of this area is lower than that of the narrow part. This is because, except for Zone I (the spray ring zone), where the entire steel strand is cooled by water sprays, only the wide part of the steel strand is cooled by the sprays in other zones.

After exiting the mold and in the spray ring zone (Zone I), the temperature initially increases. This temperature rise is due to the fact that the heat flux from the center to the surface is greater than the heat removal flux by the water spray. This temperature increase (reheating) is approximately 170 ˚C. The surface temperature reaches a maximum value determined by the equilibrium between internal heat supply and external cooling, after which it gradually decreases. When the water spray is stopped in Zone VII, the slab temperature rises again due to reduced heat removal, with a reheating effect of about 50 ˚C. Subsequently, the temperature decreases gradually until the slab is cut.

unlike the temperature variations in the wide part of the slab, there are no significant temperature changes on the surface of the narrow part. This is due to impingement of the superheated jet on the narrow face, which remelts the solidified layer near the mold's upper region. After exiting the mold and entering Zone I, a temperature jump of 100 ˚C occurs. On the narrow face, spray cooling is discontinued beyond this zone, and heat transfer occurs exclusively through radiation. After Zone I, the temperature gradually decreases.

Fig. 6. shows the variation in the solidified shell thickness along the longitudinal line.

As observed, the shell thickness stabilizes at a distance of 20.6 m from the meniscus, reaching its final value. Given that the slab thickness is 200 mm, the solidification process is complete once the thickness of the solidifying shell reaches half of this value, i.e., 100 mm Thus, the metallurgical length in this case is approximately 20.6 m.

Some metallurgical length values at different casting speeds, obtained using the numerical method, are presented in Table 3.

These values were utilized to train the Support Vector Machine (SVM) model. In total, 30 distinct datasets were used in train in SUPPORT Vector Machine (SVM).

Fig. 7. compares the metallurgical length predictions under varying casting speeds using three approaches: (1) empirical data from the casting machine (derived from the K-factor formula with 27 mm/min$^{1/2}$, (2) numerical simulation results, and (3) SVM predictions.

The mean square error (MSE) of metallurgical length predictions using the SVM method, compared to the numerical data it was trained on, is 0.0789, while the MSE relative to the empirical formula is 0.5353.

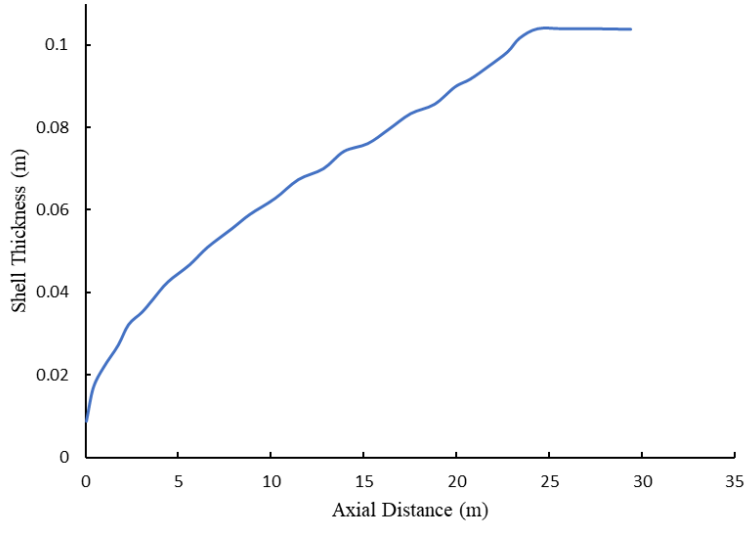

Fig. 6. Variations in Solidified Shell Thickness Along Longitudinal Line.

Table 3. Metallurgical length values at various casting speeds.

Casting Speed (m/min)	0.8	0.9	1.0	1.1	1.2	1.3	1.4
metallurgical length (m)	16.1	18.4	20.6	22.8	25.1	27.3	29.5

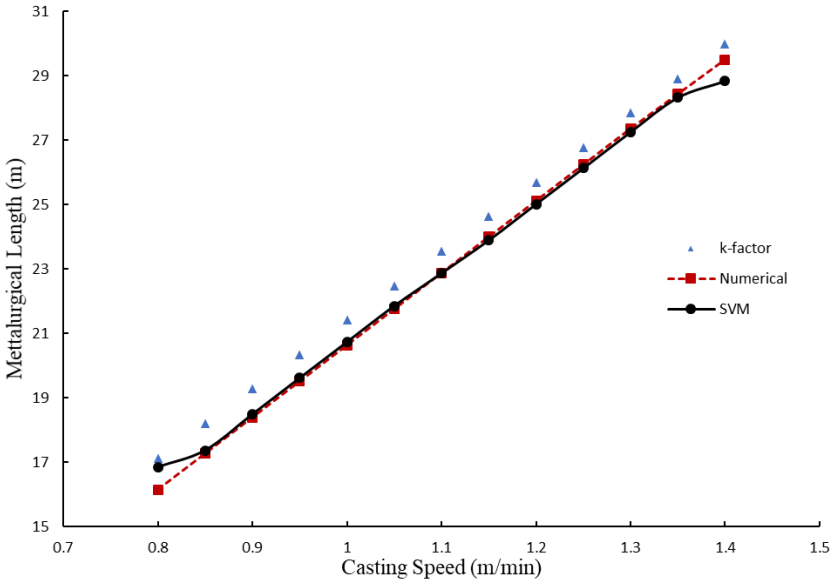

Fig. 7. Comparison of metallurgical lengths at different casting speeds for numerical, empirical, and SVM Methods.

Given the very small error associated with the SVM method, this approach can reliably be used to predict the metallurgical length in continuous casting machines. Moreover, the effects of other parameters, such as cooling water flow rate, initial superheat temperature, and other influential factors on metallurgical length, can be examined using this method.

5. Conclusions

This study successfully demonstrated the application of Support Vector Machines (SVM) for predicting metallurgical length in continuous casting, addressing the limitations of traditional methods such as the K-factor model and numerical simulations. The SVM model, trained on data from validated numerical simulations, achieved remarkable accuracy with a mean square error (MSE) of 0.0789, outperforming empirical methods. The results underscore the potential of machine learning to provide real-time, precise predictions of metallurgical length, which is critical for optimizing product quality and process efficiency in steel production.

References

[1] Petrus B, et al. New method to measure metallurgical length and application to improve computational models, Iron Steel Technol. 2015; 12(12): 58–66.
[2] Chen Y, Li G.J, Yang S.B, Zhu M.Y, Dynamic soft reduction for continuously cast rail bloom, J Iron Steel Res Int. 2007; 14(5): 13–7.
[3] Chen Z, Bentsman J, Thomas B.G, Matsui A, Study of spray cooling control to maintain metallurgical length during speed drop in steel continuous casting, Iron Steel Technol. 2017; 14(10): 92–103.
[4] Miłkowska-Piszczek K, Dziarmagowski M, Buczek A, Pióro J, The methods of calculating the solidifying strand shell thickness in a continuous casting machine, Arch Mater Sci Eng. 2012; 57(2): 75–9.
[5] Li W, Li Y, Zhang Y, Study of mould breakout prediction technique in continuous casting production, In: 2010 3rd International Conference on Biomedical Engineering and Informatics. IEEE; 2010.
[6] Cheng J, et al. Molten steel breakout prediction based on genetic algorithm and BP neural network in continuous casting process. In: Proc 31st Chinese Control Conf. IEEE; 2012.
[7] He F, Zhang L, Mold breakout prediction in slab continuous casting based on combined method of GA-BP neural network and logic rules, Int J Adv Manuf Technol. 2018; 95: 4081–9.
[8] Lu Z, et al. Real-time prediction and adaptive adjustment of continuous casting based on deep learning, Commun Eng. 2023; 2(1): 34.
[9] Cemernek D, et al. Machine learning in continuous casting of steel: A state-of-the-art survey, J Intell Manuf. 2022: 1–19.
[10] Safaei H, Emami M.D, Jazi H.S, Mostaghimi J, Application of compressible volume of fluid model in simulating the impact and solidification of hollow spherical ZrO_2 droplet on a surface, J Therm Spray Technol. 2017; 26: 1959–81.
[11] Voller V.R, Prakash C, A fixed grid numerical modelling methodology for convection-diffusion mushy region phase-change problems, Int J Heat Mass Transf. 1987; 30(8): 1709–19.
[12] Rösler F, Brüggemann D, Shell-and-tube type latent heat thermal energy storage: numerical analysis and

comparison with experiments, Heat Mass Transf. 2011; 47(8): 1027–33.
[13] Bai H, Thomas B.G, Turbulent flow of liquid steel and argon bubbles in slide-gate tundish nozzles: Part I, model development and validation, Metall Mater Trans B. 2001; 32: 253–67.
[14] Brimacombe J, Samarasekera I, Lait J, Continuous Casting. Vol. II: Heat Flow, Solidification and Crack Formation, Iron Steel Inst/AIME; 1984: 238.
[15] Vapnik V.N, Vapnik V, Statistical learning theory. 1998.
[16] Smola A.J, Schölkopf B, A tutorial on support vector regression, Stat Comput. 2004; 14: 199–222.
[17] MRRI S, Three dimensional turbulent fluid flow and heat transfer mathematical model for the analysis of a continuous slab caster, ISIJ Int. 2007; 47(3): 433–42.